Sensors and Materials, Vol. 37, No. 9 (2025) 4297–4308
MYU Tokyo

S & M 4182

Design a Multiplanar Metamaterial Solar Absorber Using COMSOL

Chia-Te Liao,[1] Kao-Peng Min,[2*] Yu-Chen Tsai,[3]
Walter Water,[4] Chi-Ting Ho,[5] and Cheng-Fu Yang[3,6**]

[1]Department of Aviation Communication and Electronics, Air Force Institute of Technology, Kaohsiung 820, Taiwan
[2]College of Engineering, National Formosa University, Huwei, Yunlin 632, Taiwan
[3]Department of Chemical and Materials Engineering, National University of Kaohsiung, Kaohsiung 811, Taiwan
[4]Department of Electronic Engineering, National Formosa University, Yunlin 632, Taiwan
[5]Department of Mechanical Design Engineering, National Formosa University, Yunlin 632, Taiwan
[6]Department of Aeronautical Engineering, Chaoyang University of Technology, Taichung 413, Taiwan

(Received September 3, 2025; accepted September 12, 2025)

Keywords: metamaterial, multiplanar absorber, ultra-broadband absorber, high absorptivity

Designing an all-planar metamaterial optical absorber that operates efficiently across a broad spectral range, from visible to infrared wavelengths, presents significant challenges due to the inherent difficulty of simultaneously achieving broadband coverage and high absorptivity using planar architectures. The core innovation of this study lies in the strategic use of cost-effective, earth-abundant materials to construct a high-performance optical absorber capable of covering the entire spectral range from 400 to 1980 nm. Unlike conventional approaches that often rely on expensive noble metals such as gold and silver, this work utilized more affordable alternatives—namely, copper (Cu), nickel (Ni), chromium (Cr), and titanium (Ti), and two different dielectric materials SiO_2 and MgF_2—to design a multilayer, planar metamaterial structure. These metals were selected not only for their economic viability but also for their distinct optical and physical properties, which, when combined in an optimized configuration, contributed to superior absorption characteristics. The proposed absorber demonstrated an impressive ultra-broadband performance, with an absorptivity consistently exceeding 0.9 throughout the visible and near-infrared range. Its average absorptivity reached as high as 0.979, and a peak absorptivity of 0.999 was recorded at certain wavelengths, effectively qualifying the device as a near-perfect absorber. Such high performance is rarely observed in planar structures composed solely of low-cost materials, underlining the novelty and practical significance of the design.

1. Introduction

Photon-trapping layers are specially engineered materials designed to enhance light absorption within photovoltaic devices, particularly in solar cells. These layers significantly boost the efficiency of solar energy conversion by confining and manipulating incident light

*Corresponding author: e-mail: D1481103@nfu.edu.tw
**Corresponding author: cfyang@nuk.edu.tw
https://doi.org/10.18494/SAM5923

within the active semiconductor region. Through mechanisms such as light scattering, resonance enhancement, and refractive index modulation, photon-trapping layers enable solar cells to harvest more sunlight and convert it into electricity more effectively. Their capability to localize and prolong light–matter interactions in the absorbing medium is especially critical for thin-film and next-generation photovoltaic technologies, where maximizing light absorption in limited material volumes is essential. To this end, a growing body of research has focused on the development of absorber structures with ultra-broadband absorption characteristics, those capable of achieving high absorptivity across an expansive spectral range, from the visible to infrared region.[1,2] Such broad-spectrum absorbers are crucial not only for improving solar cell performance but also for applications in photodetectors, thermal emitters, and energy harvesting devices.

Optical absorbers play a pivotal role in diverse sensing applications, where their detection mechanisms rely on several fundamental physical effects.[3] For instance, in gas sensing, the absorption spectrum of certain materials shifts in response to the presence of a specific gas such as NO_2, H_2S, or CO_2, enabling the accurate identification and quantification of target analytes.[4] In the biomedical field, nano-optical absorbers, such as gold nanorods, are employed to detect proteins, DNA, or cellular interactions. These devices operate by monitoring variations in optical absorption characteristics that occur when biomolecules bind to the absorber surface. Similarly, photothermal absorbing materials are highly sensitive to temperature fluctuations, making them particularly suitable for noncontact thermal imaging and thermal radiation detection. Moreover, optical absorbers enhance the performance of advanced imaging techniques, including high-sensitivity optical imaging and dark-field microscopy, by improving contrast and facilitating the detailed visualization of microscopic structures.[5] Recent efforts aim to push the limits of light trapping efficiency by designing nearly perfect absorbers that can operate under various environmental and angular conditions.

For example, Ding *et al.* introduced a polarization-independent ultra-broadband metamaterial absorber based on a periodic array of multilayered quadrangular frustum pyramids, each engineered to support multiple absorption modes across different wavelengths.[6] This hierarchical design enables the efficient coupling of incident light into plasmonic and dielectric resonances, resulting in near-perfect absorption over a wide frequency spectrum. Their work exemplifies the potential of metamaterials to achieve tailored optical responses through structural and material innovation, offering new directions for broadband absorber design. As research in this area progresses, future absorber technologies will likely emphasize not only spectral and angular robustness but also material cost-effectiveness, fabrication scalability, and integration compatibility with existing photovoltaic platforms. These developments will pave the way for the next generation of high-efficiency, multifunctional optoelectronic devices and sensors. Planar optical absorbers offer several distinct advantages over more complex or bulky absorber architectures, making them highly attractive for modern photonic and optoelectronic applications.[7]

(a) First, their inherently compact and space-efficient structure allows for deployment in environments with a limited installation area, enabling seamless integration into a wide range of systems, from microscale photonic circuits to large-area solar harvesting modules.

(b) Second, the simplicity of planar designs lends itself to straightforward nanofabrication processes, such as sputtering, atomic layer deposition, and electron-beam lithography. These fabrication techniques support large-scale manufacturing while maintaining low production costs, which is critical for the commercialization of advanced absorber technologies.
(c) Moreover, the combination of structural compactness and ease of production enhances the compatibility of planar absorbers with various optical and optoelectronic devices, including photodetectors, sensors, and infrared imaging systems. This integration potential makes planar absorbers especially suitable for multifunctional and miniaturized device platforms.
(d) In addition to their structural and manufacturing advantages, planar optical absorbers are highly adaptable and can be engineered for targeted applications through the careful tuning of material composition, geometric configuration, and layer thickness. This tunability enables designers to tailor the absorber's spectral response and electromagnetic characteristics, facilitating ultra-broadband absorption performance across visible, near-infrared, and even mid-infrared regions. The incorporation of multilayer structures further extends this capability, allowing controlled interference, resonance, and dispersion management to maximize light absorption over a broad spectral range.

A particularly effective strategy in optimizing planar absorbers is impedance matching, wherein the structure is designed to match the optical impedance of free space. This approach minimizes reflection losses at the air–absorber interface and enhances the transfer of incident electromagnetic energy into the absorber. By combining impedance-matching principles with multilayer engineering, we can realize strong, consistent, and broadband absorption characteristics, which are key attributes for high-performance energy harvesting, thermal emission control, and sensing technologies. Designing efficient planar light absorbers presents a number of technical challenges that must be carefully addressed to achieve high optical performance. One major limitation is the restricted light propagation within planar geometries, which inherently reduces the interaction length between incoming photons and the absorbing medium, thereby limiting overall absorption efficiency. Additionally, surface reflection at the air–material interface results in a significant portion of incident light being lost before it can penetrate the active region. Furthermore, intrinsic optical losses—stemming from material scattering, parasitic absorption, and imperfect interfaces—can further degrade the device's capability to harvest or convert light effectively.

There are numerous approaches to designing ultra-broadband optical absorbers. In our previous research, we employed multilayer structures, where not all layers were planar, to fabricate ultra-broadband optical absorbers. The design incorporated two intermediate layers consisting of noncontinuous planar Fe structures, with the topmost layer featuring a discontinuous cylindrical Ti matrix.[8] Although this design approach demonstrated the feasibility of utilizing cost-effective metallic and nonmetallic materials, it presented significant manufacturing challenges due to the complexity of fabricating nonplanar and discontinuous structures. The fabrication difficulties associated with noncontinuous and three-dimensional geometries include the precise alignment of multiple layers, maintaining structural integrity during assembly, and achieving reproducible optical properties across large-scale production. Our ongoing research efforts aim to demonstrate that continuous planar structures offer

substantial advantages in terms of manufacturability, scalability, and cost-effectiveness. Therefore, this research focuses on developing an all-planar structural design to achieve the required ultra-broadband optical absorption characteristics. By utilizing only continuous planar layers, we expect to maintain the desired broadband absorption performance while significantly simplifying the manufacturing process and reducing production complexity.

To overcome these limitations, it is crucial to optimize both the geometric structure and material composition of the absorber. This includes fine-tuning the thickness of each absorption layer to achieve constructive interference effects, enhance optical path length, and minimize reflection. Equally important is the implementation of carefully engineered optical structures that can leverage resonant phenomena, such as the Fabry–Pérot resonance and plasmonic effects, to boost absorptivity across a wide spectral range. In this study, we focus on the design and performance analysis of an eight-layered planar metamaterial absorber, specifically targeting UWB absorption from the visible to near-infrared (NIR) region. Through the rigorous simulation and optimization of layer materials, thicknesses, and refractive index contrasts, the proposed structure was engineered to maximize light confinement and absorption efficiency. The final design achieved an absorptivity exceeding 0.9 across the broad spectral range of 400 to 1980 nm, with a peak absorptivity of 0.999, effectively exhibiting the behavior of a near-perfect absorber. These results validate the effectiveness of the multilayer configuration in overcoming the inherent technical challenges in manufacturing planar absorbers and underscore its potential for applications in solar energy harvesting, photodetection, and thermal emission control.

2. Methodology

To achieve ultra-broadband and high-efficiency light absorption, we conducted a series of comprehensive numerical simulations and analyses on a carefully designed multilayer thin-film structure. The simulation work was carried out using COMSOL Multiphysics® (version 6.0), a highly reliable and widely adopted finite element method (FEM) software platform. Previous studies have consistently confirmed the accuracy and robustness of COMSOL for modeling nanophotonic and optoelectronic systems, particularly in evaluating the electromagnetic performance of complex layered absorbers.[9,10] By leveraging COMSOL's advanced computational capabilities, we were able to precisely model the optical behavior of the proposed metamaterial absorber across a wide spectral range. The structure under investigation is illustrated in Fig. 1 and comprises a vertically stacked, multiplanar configuration designed to optimize light absorption from the visible to NIR region. Each of the eight layers was arranged sequentially from bottom to top, with material selection and thickness precisely optimized through an iterative parameter-scanning method to achieve maximum absorptivity. The materials used include metals such as copper (Cu), nickel (Ni), chromium (Cr), and titanium (Ti), interleaved with dielectric layers of silicon dioxide (SiO_2) and a top antireflective layer of magnesium fluoride (MgF_2). The final optimized thicknesses were as follows: Cu (200 nm), SiO_2 (70 nm), Ni (7 nm), SiO_2 (50 nm), Cr (5 nm), SiO_2 (100 nm), Ti (5 nm), and MgF_2 (110 nm), with the overall lateral width of the structure set at 200 nm.

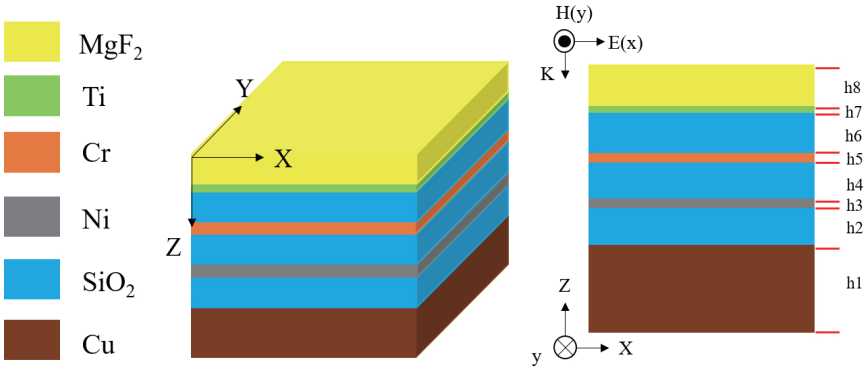

Fig. 1. (Color online) 3D and side views of the investigated planar absorber.

To accurately capture the complex optical interactions, including interference, resonance, and plasmonic effects occurring at the interfaces, a high-quality mesh was generated for the simulation domain. The mesh comprised a total of 780 grid nodes, with grid lengths ranging from 1.2 to 2.2 nm, allowing the model to resolve fine-scale optical field variations effectively. The meshing strategy incorporated a mixture of endpoint elements (22), edge finite elements (268), standard finite elements (272), and triangular elements (1,254). This fine and diverse meshing ensured both numerical stability and high-resolution computation, essential for modeling broadband electromagnetic responses. Furthermore, the mesh quality was quantitatively assessed to ensure the reliability of simulation results. The average element quality reached 0.8282 and the minimum quality was 0.5521, indicating a well-constructed mesh with minimal distortion and excellent numerical conditioning. The model was configured to simulate the interactions of electromagnetic waves within a wavelength range of 300 to 3000 nm, fully covering the visible and NIR bands and extending into the mid-infrared region. This broad spectral coverage aligns closely with the AM1.5G solar spectrum, making the absorber design highly relevant for practical solar energy applications. The primary objective of this simulation study was to determine the optimal combination of material layering and geometric parameters that would result in near-perfect absorptivity across the desired spectrum. By meticulously refining the structural configuration, we aimed to develop a planar optical absorber capable of efficiently harvesting solar energy by targeting the most energetic regions of sunlight, thereby maximizing its potential for integration into next-generation photovoltaic, thermophotovoltaic, and photodetection systems.

3. Simulation Results and Discussion

In this section, we focused on analyzing the effect of the thickness of each layer on the overall absorptivity of the proposed multiplanar metamaterial absorber. To systematically evaluate the contribution of each layer to the absorber's performance, we selected several key layers that were hypothesized to play a dominant role in light–matter interactions, particularly in enhancing absorption through impedance matching and resonant effects. Our approach involved varying the thickness of one target layer at a time while keeping the thicknesses of the remaining seven

layers fixed at their initially selected values. This method enabled us to isolate and quantify the impact of each layer's thickness on spectral absorptivity. As illustrated in Fig. 2(a), we first examined the effect of the second layer (h2), composed of SiO_2, by incrementally increasing its thickness from 56 to 186 nm. The simulation results reveal that changes in the thickness of h2 induce significant variations in the absorption spectrum, particularly within the wavelength ranges of 300–450 nm and beyond 2200 nm. Notably, within these spectral windows, the absorptivity consistently exceeded 0.900, underscoring the critical role of dielectric spacing in affecting interference effects and electromagnetic field confinement.

The selection of 70 nm for the h2 layer was based on a careful balance between high absorptivity across both visible and infrared regions and structural feasibility. After the fixing h2 layer thickness at 70 nm, we proceeded to optimize the thicknesses of the remaining layers. Each subsequent layer was fine-tuned to further enhance broadband absorption by leveraging the synergetic effects of Fabry–Pérot and surface plasmon resonances, and impedance matching across material interfaces. This step-by-step optimization process ensured that the final absorber configuration could achieve superior performance over a wide spectral range, from the ultraviolet and visible to NIR regions. Through this iterative parameter refinement, we demonstrated that small variations in individual layer thicknesses, particularly those of dielectric interlayers, can lead to considerable improvements in absorptivity. These findings highlight the sensitivity of multiplanar absorber designs to nanoscale geometric tuning and emphasize the importance of precision control in nanofabrication for achieving ultra-broadband absorption.

Figure 2(b) illustrates the effect of varying the thickness of the h5 layer, composed of Cr, on the absorption performance of the proposed multiplanar metamaterial absorber. When the h5 layer thickness was gradually increased from 2 to 50 nm, a pronounced reduction in broadband absorptivity was observed. This reduction was manifested as a progressive narrowing of the spectral region in which the absorptivity remained above 0.900, indicating that excessive Cr thickness deteriorates the absorber's capability to sustain broadband performance. The effect was particularly evident in the NIR region: once the thickness exceeded 10 nm, the absorptivity beyond 1500 nm dropped sharply, signifying the stronger reflection and weakened confinement of incident light. This phenomenon can be attributed to the dual role of the Cr layer. On one hand, a sufficiently thin metallic layer facilitates localized surface plasmon resonance, thereby enhancing light–matter interactions and promoting strong absorption. On the other hand, excessive thickness introduces higher optical losses and reflectivity, which in turn suppresses the resonance effect and diminishes broadband absorption efficiency. As a result, the Cr layer does not act merely as a passive component but critically governs the balance between plasmonic excitation and dissipative losses. Through this analysis, a thickness of approximately 5 nm was identified as optimal. At this value, the Cr layer is sufficiently thick to sustain plasmonic excitation while thin enough to minimize parasitic reflection and absorption losses. Consequently, the absorber maintains strong light confinement and high broadband absorptivity, demonstrating that the precise control of metallic layer thickness is essential for achieving superior optical performance in multilayer metamaterial absorbers.

On the basis of Fig. 2(c), we explore the effect of the thickness of the h6 layer, which corresponds to the third SiO_2 dielectric layer in the stack. The thickness of this layer was varied

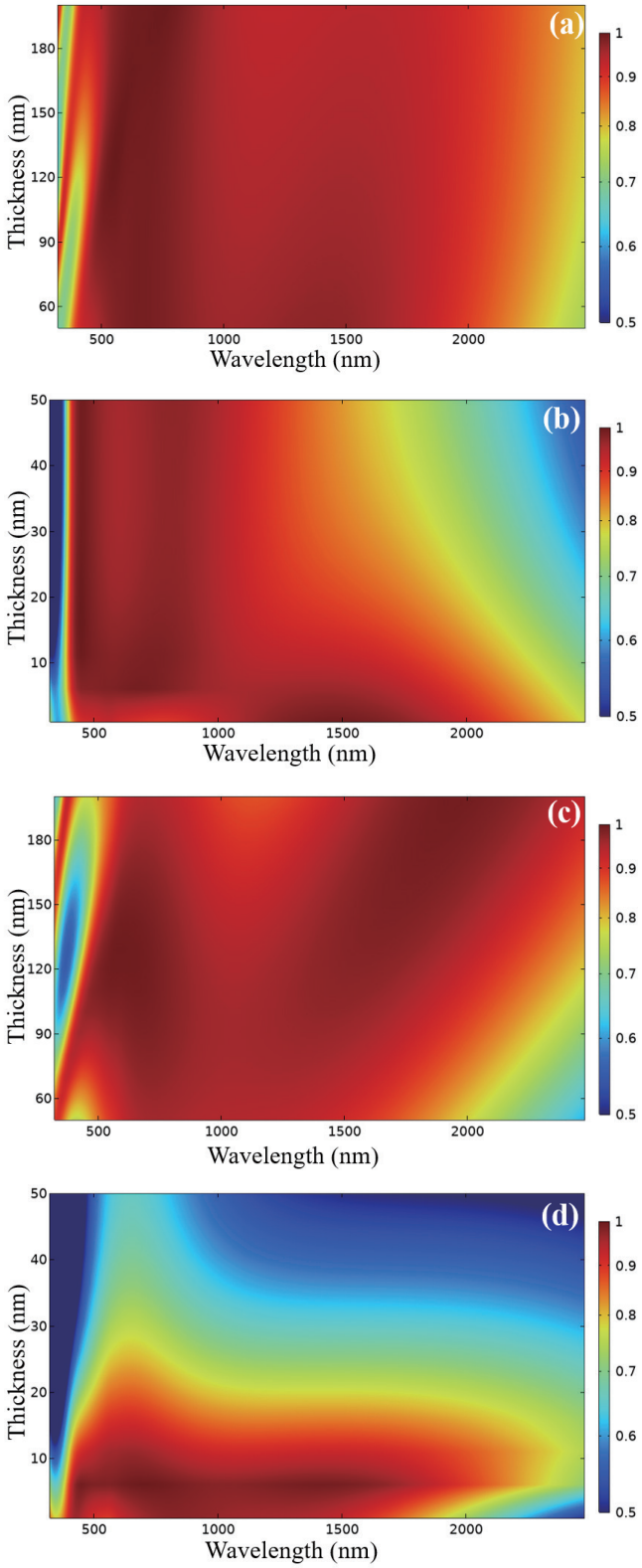

Fig. 2. (Color online) Effects of various simulation wavelengths and thicknesses of (a) h2, (b) h5, (c) h6, and (d) h7 layers on the absorptivity distributions of the investigated planar absorber.

from 50 to 195 nm to evaluate its effects on spectral absorptivity and resonance distribution. As the thickness exceeded 65 nm, a distinct green-blue region, indicative of lower absorptivity, began to emerge within the wavelength range of 300–500 nm. This absorptivity dip gradually shifted to longer wavelengths as the h6 layer thickness increased further, surpassing 105 nm. Conversely, when the layer was thinner than 75 nm, the green-blue region shifted toward the ultraviolet region, appearing below 200 nm. These results suggest that the h6 layer critically affects the interference conditions within the absorber and modulates constructive and destructive interference patterns across the spectrum. Given that our target is to sustain absorptivity above 0.900 across the 400–2000 nm range, aligning with the most energy-dense region of the solar spectrum, a thickness of 100 nm for the h6 layer was identified as optimal. This configuration effectively suppresses low-absorptivity regions and maximizes overall efficiency.

As shown in Fig. 2(d), we investigated the effect of varying the thickness of the h7 layer consisting of Ti from 2 to 50 nm. The results reveal that the presence of high-absorptivity red-orange regions, typically signifying enhanced plasmonic coupling, only occurred when the thickness was below 16 nm. Notably, as the h7 layer thickness decreased from 16 to 2 nm, these red-orange regions exhibited a blue shift, moving from 2250 to approximately 1800 nm. This behavior highlights the sensitivity of surface plasmon resonance to subwavelength-scale changes in metal thickness, particularly in the NIR region. Thin Ti layers in this range act as efficient plasmonic materials that amplify field confinement and absorption. Therefore, a thickness of 5 nm for the h7 layer was selected to ensure strong resonance in the desired spectral range while minimizing ohmic losses. Collectively, these layer-by-layer optimizations underscore the crucial role of individual material thicknesses in tailoring the absorber's spectral response. The selected configuration, consisting of h5 = 5 nm, h6 = 100 nm, and h7 = 5 nm, in conjunction with fine-tuned parameters for the remaining layers, enabled the realization of a high-performance, ultra-broadband absorber. This structure achieves enhanced light harvesting across a broad spectral window, making it suitable for applications in solar energy conversion, thermal photonics, and optoelectronic integration.

To evaluate the effect of structural complexity on absorption performance, absorbers comprising 3, 5, and 8 layers were modeled and analyzed, with the results presented in Fig. 3(a). The simplest configuration, consisting of 3 layers, formed a basic resonant cavity. This setup yielded a distinct absorption peak at approximately 450 nm, primarily attributed to the Ni layer (h3), which effectively absorbs light in the blue portion of the spectrum. When the structure was expanded to 5 layers, the absorption behavior evolved owing to additional interference effects introduced by the newly inserted dielectric and metallic layers. In this configuration, the absorption peak of the Ni layer red-shifted to around 500 nm, whereas a new peak emerged at approximately 930 nm, corresponding to the Cr layer (h5). These shifts suggest enhanced interactions and coupling among the multilayer elements, increasing the spectral range of effective light trapping. Further extending the structure to 8 layers introduced additional plasmonic and cavity resonance effects. In this full configuration, the absorption peaks of the h3 and h5 layers blue-shifted to approximately 400 and 800 nm, respectively, owing to altered optical path lengths and field distributions across the increased number of interfaces. Moreover,

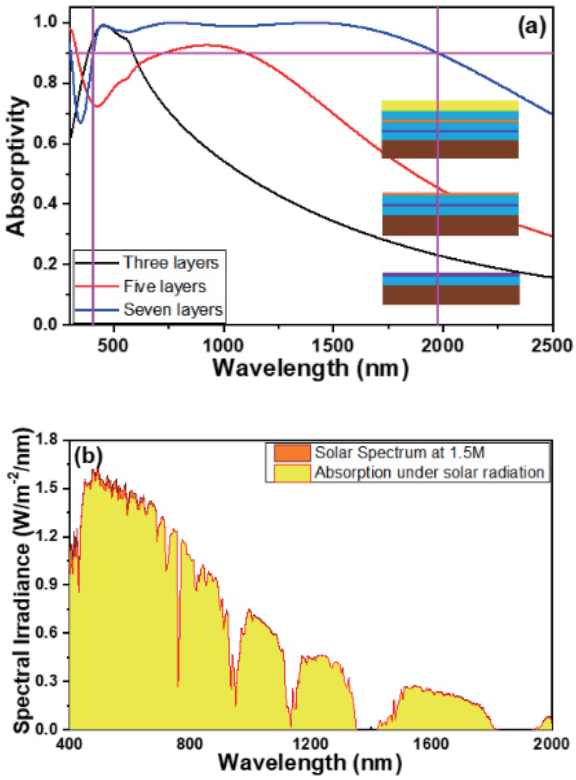

Fig. 3. (Color online) (a) Effect of different structures on the absorption spectra and (b) absorption spectrum of the investigated absorber under the AM1.5 solar spectrum.

a new absorption peak emerged at 1400 nm, attributed to the Ti layer (h7), which supports plasmonic resonance in the NIR range. The presence of multiple absorption peaks spanning a wide range of wavelengths indicates that the multilayer structure promotes broadband absorption through the superposition of distinct resonance modes, including the Fabry–Pérot interference and surface plasmon resonance.

To further verify the efficiency of the absorber under practical illumination conditions, we simulated its spectral response under the AM1.5 global solar spectrum, as shown in Fig. 3(b). The results revealed that the absorber achieved outstanding absorptivity across key solar spectral bands: 74.6% in the ultraviolet range (280–400 nm), 97.7% in the visible range (400–700 nm), 99.5% in the near-infrared range (700–1400 nm), and 93.1% in the extended NIR region (1400–3000 nm). Beyond 3000 nm, absorptivity dropped to 40.7%, as the energy contribution from this spectral region under solar illumination is minimal. Importantly, the average absorptivity across the 400–2000 nm range reached 97.9%, underscoring the absorber's effectiveness across the most energy-rich portion of the solar spectrum. A maximum absorptivity of 0.999 was also recorded, demonstrating the absorber's near-perfect performance at its peak wavelength. These results affirm that the majority of the absorption occurs within the visible to near-infrared spectrum, which aligns closely with the spectral distribution of solar energy. Thus, the proposed multiplanar metamaterial absorber exhibits excellent potential for high-efficiency solar energy harvesting, thermal photonic applications, and integration into photovoltaic systems, where

maximizing light absorption across a broad spectrum is critical.

We conducted a detailed analysis of the magnetic field distributions at key wavelengths of 450, 800, and 1400 nm, as illustrated in Fig. 4(a). At a wavelength of 450 nm, strong magnetic field concentration was observed within the SiO_2 layer (h6), confirming the excitation of the Fabry–Pérot cavity resonance within the absorber structure. This resonance effect plays a pivotal role in enhancing light absorption by trapping light within the cavity, which results in significant field enhancement. At all three wavelengths—450, 800, and 1400 nm—the strong magnetic field distributions were predominantly located at the surface of the multilayer structure. This behavior is indicative of surface plasmon resonance, which is known for its capability to

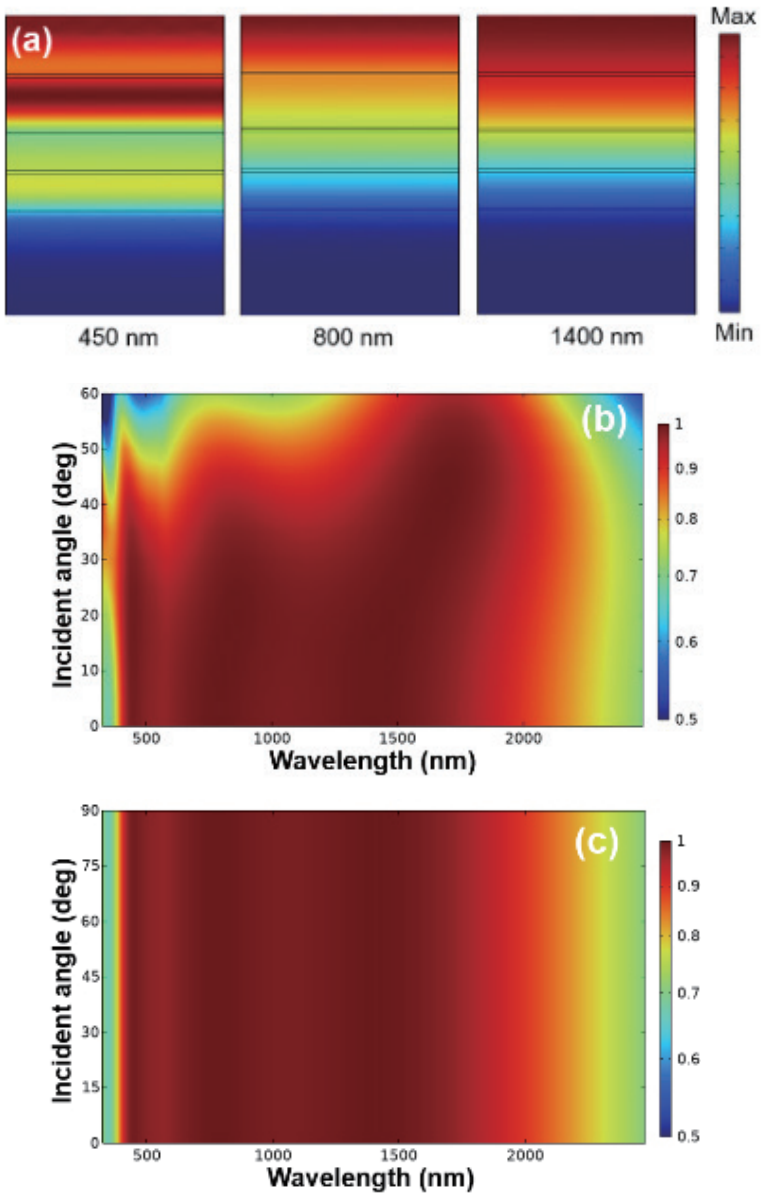

Fig. 4. (Color online) (a) Distributions of the magnetic field intensities at different wavelengths and absorptivity distributions of (b) TE-polarized and (c) TM-polarized light with various oblique incidence angles.

concentrate electromagnetic fields at metal–dielectric interfaces, further boosting the absorption capability of the material. The distributions of electric fields showed similar patterns to those of magnetic fields, with enhanced electric fields also localized at the interfaces and confirming the joint contribution of the Fabry–Pérot and surface plasmon resonances to the overall absorption mechanism. This overlap of the Fabry–Pérot and surface plasmon resonances is thus primarily responsible for the absorption peaks observed at the specified wavelengths.

In addition to these analyses, we evaluated the absorption performance of the designed multilayer absorber with respect to the light incident angle varied from 0 to 90°, to assess its angular tolerance and stability. As shown in Fig. 4(b), under transverse electric (TE) polarization, the absorber demonstrated absorptivity exceeding 0.900 for light incident angles between 0° and approximately 40 to 60° across the 400–2000 nm wavelength range. This behavior highlights the absorber's high performance over a range of typical light incident angles. In contrast, under transverse magnetic (TM) polarization, as illustrated in Fig. 4(c), the absorber's absorptivity above 0.900 extended gradually from 0 to 90°, effectively covering a wider range of light incident angles. The simulation results in Figs. 4(b) and 4(c) underscore the fact that the absorber maintains high efficiency (above 0.900 absorptivity) across various light incident wavelengths and angles, indicating its robustness and suitability for practical applications, where light incidence may not always be normal to the surface. These findings demonstrate that the multilayer ultra-broadband absorber designed in this study is highly insensitive to changes in light incident angle, making it an excellent candidate for diverse applications, such as photovoltaic systems or thermal management devices, where angular tolerance and efficient energy absorption are critical. The combination of the Fabry–Pérot and surface plasmon resonances, coupled with the absorber's broad response across both visible and infrared wavelengths, confirms its high absorption performance and potential for wide-ranging applications in solar energy harvesting, photonic sensing, and thermal radiation control.

4. Conclusions

The 3-layer structure of the absorber initially created a basic resonant cavity, with the absorption peak for the Ni layer (h3) observed at 450 nm. As the configuration evolved to a 5-layer design, this absorption peak shifted to 500 nm, whereas the Cr layer (h5) introduced a new absorption peak at 930 nm. With further extension of the structure to 8 layers, the absorption peaks for the Ni (h3) and Cr (h5) layers shifted to 400 and 800 nm, respectively. Additionally, the Ti layer (h7) exhibited a new absorption peak at 1400 nm. This multilayer setup facilitated the tuning of absorption peaks across a wide range of wavelengths, illustrating the potential for customizing the absorber's spectral response. In terms of resonance effects, at a wavelength of 450 nm, a strong magnetic field was observed within the SiO_2 layer at the h6 layer, confirming the activation of the Fabry–Pérot cavity resonance. The presence of the Fabry–Pérot resonance contributed significantly to light trapping and enhanced absorption within the cavity. Moreover, for wavelengths of 450, 800, and 1400 nm, the strong magnetic field distribution was localized at the surface of the structure, a clear indication of surface plasmon resonance at the metal–dielectric interfaces. Surface plasmon resonance further amplified the absorber's performance

by concentrating electromagnetic fields at these interfaces, thereby increasing energy absorption. When evaluated across the solar spectrum, the absorber demonstrated outstanding absorptivity. The absorptivity values were 74.6% in the 280–400 nm range, 97.7% in the 400–700 nm range, 99.5% in the 700–1400 nm range, 93.1% in the 1400–3000 nm range, and 40.7% in the 3000–4000 nm range. Notably, the average absorptivity from 400 to 2000 nm reached 97.9%, underscoring the absorber's high performance within the crucial wavelength range of visible to near-infrared light. The designed absorber achieved a peak absorptivity of 0.999 and consistently maintained an absorptivity greater than 0.9 across the 400–1980 nm range. This performance illustrates the exceptional effectiveness of the multilayer absorber, making it a near-perfect optical absorber for harnessing solar energy within the AM1.5G solar spectrum. These results affirm the absorber's potential for solar energy applications, where broad-spectrum absorption and high efficiency are crucial for maximizing energy capture. The combination of the Fabry–Pérot and surface plasmon resonances, along with the optimized multilayer design, demonstrates its promise as a highly efficient and versatile optical absorber.

Acknowledgments

This work was supported by Summit-Tech Resource Corp. and projects under Nos. NSTC 113-2221-E-390-011 and NSTC 113-2221-E-005-042, and the funding of the Ministry of National Defense of the Taiwan under the 2025 Military Instructor Research Grant. We would like to thank Pitotech Co., Ltd. for teaching the use of COMSOL Multiphysics® software.

References

1 G. Peng, W. Z. Li, L. C. Tseng, and C. F. Yang: Nanomaterials **13** (2023) 766.
2 G. Peng, P. X. Ke, L. C. Tseng, C. F. Yang, and H. C. Chen: Photonics **10** (2023) 804.
3 X. Liu, K. Li, Z. Meng, Z. Zhang, and Z. Wei: Front. Phys .**9** (2021) 637602.
4 Y. E. Monfared and M. Qasymeh: Results Phys. **23** (2021) 103986.
5 M. L. Hakim, A. Hanif, T. Alam, M. T. Islam, H. Arshad, M. S. Soliman, S. M. Albadran, and Md. S. Islam: Nanomaterials **12** (2022) 2849.
6 F. Ding, Y. Cui, X. Ge, Y. Jin, and S. He: Appl. Phys. Lett. **100** (2012) 103506.
7 A. E. Assal, H. Breiss, R. Benzerga, and A. Sharaiha: J. Mater. Sci. **56** (2021) 19484.
8 L. Wang, C. M. Ho, C. T. Chen, C. F. Yang, and K. W. Min: Sens. Mater. **37** (2025) 3697.
9 H. Akafzade and S. C. Sharma: AIP Adv. **10** (2020) 035209.
10 J. J. Lin, D. Y. Huang, M. L. Hong, J. L. Huang, C. H. Wang, C. F. Yang, and K. K. Lai: Photonics **11** (2024) 939.